Defects and transport in langasite I: Acceptor-doped (La$_3$Ga$_5$SiO$_{14}$)

H. Seh · H. L. Tuller

Abstract Both nominally undoped and 1%Sr-doped langasite were found to exhibit acceptor behavior and correspondingly mixed ionic-electronic conductivity under experimentally accessible conditions. At high pO$_2$, the conductivity of nominally undoped langasite was pO$_2$-independent (ionic behavior) but became increasingly pO$_2$-dependent (n-type behavior) under reducing conditions. The substitution of strontium on lanthanum sites, increased the ionic and introduced a p-type electronic conductivity behavior at the highest pO$_2$'s, while completely depressing the n-type electronic conductivity – observations consistent with predictions of the proposed defect model based on oxygen vacancy formation in response to negatively charged acceptor impurities.

Sr-doped langasite was found to have a higher activation energy for oxygen ion transport (1.27 ± 0.02 eV) than nominally undoped langasite (0.91 ± 0.01 eV). This difference could not be successfully explained by applying a simple defect association model but required the assumption of long range defect interactions.

Using the defect model, a number of key equilibrium constants (reduction (5.7 ± 0.06 eV), oxidation (2.18 ± 0.08 eV), electron-hole generation (3.94 ± 0.07 eV), and defect mobilities (oxygen vacancies and holes) were derived and summarized.

Keywords Resonator · Defect equilibria · Electrical properties · Mixed ionic-electronic conductor

H. Seh (✉)· H. L. Tuller
Crystal Physics and Electroceramics Laboratory, Department of Materials Science and Engineering, Massachusetts Institute of Technology, Cambridge, MA 02139, USA

Introduction

Langasite, which retains its piezoelectric properties to elevated temperatures, has operated as a surface acoustic wave device to temperature as high as 1000°C [1], greatly surpassing the temperature limitations of other piezoelectric materials [2]. The high temperature capabilities of langasite, for example, make it a prime candidate as a crystal microbalance-based sensor for in-situ monitoring of e.g., automobile exhaust [3–5]. This not only requires that langasite retain its piezoelectric properties to high temperatures, but that it also remain stable in atmospheres ranging from highly reducing to oxidizing. In addition to chemical stability, electrical and mechanical losses must be minimized to prevent loss of sensor resolution and hence sensitivity [6]. Consequently, the ability to characterize and ultimately predict the electrical behavior and transport properties of langasite at elevated temperatures and over a wide oxygen partial pressure range is crucial.

Previously, in [7–9], brief preliminary descriptions of langasite's defect chemistry were reported. However, key parameters, including carrier mobilities, were unavailable to enable a complete description of the defect equilibria. Furthermore, certain assumptions regarding the nature of the charge carriers, e.g. ionic versus electronic, were unconfirmed. Since then, complementary thermoelectric power, mass spectroscopy and concentration cells measurements have been completed, allowing for a more accurate and complete picture of the defect equilibria and transport properties of langasite to be established. In this paper, the defect chemistry and transport properties of acceptor-doped langasite are examined. Donor-doped langasite is treated in a companion paper [10]. A third paper examines how the defect and transport properties of langasite need to be controlled to achieve optimum performance in langasite-based crystal

microbalance gas sensors operating under high temperature conditions [11].

Theory

The defect structure and chemistry of materials have a significant influence on their electrical properties, with corresponding implications for electrical losses in crystal resonators. In addition, the generation of oxygen vacancies, resulting in corresponding mass changes, contributes to undesirable frequency shifts when the crystal is being used as a sensor platform. Determination of langasite's defect chemistry will therefore provide the means for understanding the origins of these changes and thereby provide the tools needed to mitigate or eliminate these superfluous effects.

Preliminary studies point to an oxygen vacancy defect model, with singly ionized acceptors playing a dominant role under most conditions [12, 13]. One can describe equilibration of the material with the gas phase by the reduction reaction under which double charged oxygen vacancies and compensating electrons are formed

$$O_O^X \rightarrow V_O^{\bullet\bullet} + 2e' + \tfrac{1}{2}O_2 \tag{1}$$

The related mass action equation is:

$$K_r = \left[V_O^{\bullet\bullet}\right] n^2 pO_2^{1/2} = k_r \exp\left(\frac{-E_r}{kT}\right) \tag{2}$$

Correspondingly, one could instead describe equilibration with the gas phase via an oxidation reaction, in which oxygen vacancies are annihilated and electron holes are generated.

$$\tfrac{1}{2}O_2 + V_O^{\bullet\bullet} \rightarrow O_o^x + 2h^{\bullet} \tag{3}$$

The related mass action equation is:

$$K_O = p^2 \left[V_o^{\bullet\bullet}\right]^{-1} pO_2^{-1/2} = k_o \exp\left(\frac{-E_O}{kT}\right) \tag{4}$$

Intrinsic ionic disorder is assumed to be based on the displacement of oxygen ions from normal to interstitial sites, i.e. the anion frenkel reaction:

$$O_O^X \rightarrow V_O^{\bullet\bullet} + O_i'' \tag{5}$$

The related mass action equation is:

$$K_F = \left[V_O^{\bullet\bullet}\right][O_i''] = k_F \exp\left(\frac{-E_F}{kT}\right) \tag{6}$$

The thermal generation and recombination of electrons and holes is represented by:

$$null \rightarrow h^{\bullet} + e' \tag{7}$$

which gives the mass action equation:

$$pn = k_i \exp\left(\frac{-E_g}{kT}\right) = N_C N_V \exp\left(\frac{-E_g}{kT}\right) \tag{8}$$

with E_g being the thermal bandgap and N_C and N_V the effective density of states in the conduction and valence bands respectively. Taking the product of Eqs. (2) and (4), one can easily demonstrate that the np product is given by:

$$\sqrt{K_r K_O} = np = \sqrt{k_r k_O} \exp\left(\frac{-(E_r + E_O)}{2kT}\right) \tag{9}$$

Hence by comparing Eqs. (8) and (9), the thermal bandgap can be related to the oxidation and reduction enthalpies:

$$E_g = \frac{E_r + E_o}{2} \tag{10}$$

and the density of states to the pre-exponential terms as:

$$N_c N_v = k_i = \sqrt{k_r k_o} \tag{11}$$

Following statistical thermodynamics, one derives expressions for the density of states given by [14]:

$$N_c = N_v = 2.5 \left(\frac{m_{e,h}^*}{m_o}\right) \left(\frac{T}{300K}\right)^{3/2} \times 10^{19} \text{ cm}^{-3} \tag{12}$$

Combining all the charged species (assuming predominantly singly-charged acceptor dopants), results in the electrical neutrality equation:

$$n + 2[O_i''] + [A'] = p + 2\left[V_O^{\bullet\bullet}\right] \tag{13}$$

Based on Eqs. (2), (4), (6), (8) and (13), it becomes possible, in principle, to determine the concentration of all charged species and their respective partial conductivities, at any temperature, oxygen partial pressure and dopant level, assuming knowledge of the respective defect mobilities. However, solving the above set of simultaneous equations is normally difficult and so the so-called Brouwer approximation is often applied, in which the neutrality and mass balance equations are simplified to include only one defect species on either side of the equality over restricted ranges of pO_2 and temperature [15–17]. Commonly, for acceptor-doped materials, four defect regions are defined: reduction, ionic compensation, electronic compensation, and oxidation. The solutions,

based on the Brouwer approximations, are summarized in Table 1 with the corresponding Kroger-Vink diagram, illustrating the characteristic pO_2-dependence of the various defect species, shown in Fig. 1.

Based on Table 1, for the defect region characterized by oxygen vacancy – acceptor dopant compensation, one predicts a $pO_2^{-1/4}$-dependence of the electron conductivity, a $pO_2^{+1/4}$-dependence of the hole conductivity and pO_2 independence of oxygen vacancy conductivity (see Region II, Fig. 1).

In order to independently confirm that the ionic conductivity dominates in certain pO_2 and temperature regimes, concentration cell measurements are used. This experiment involves measuring the open circuit voltage across a sample, exposed on one side to say a reference atmosphere such as air and the other to a different pO_2. The open circuit voltage (V) is related to the average transport number by the Eq. [18]:

$$V = \bar{t_i} \frac{kT}{4q} \ln \frac{pO_2}{pO_{2,air}}$$
(14)

where $\bar{t_i}$ is the average ionic transport number, k is the Boltzmann's constant, q is the elementary charge, and pO_2 and $pO_{2,air}$ correspond to oxygen partial pressures at the two sides of the sample. To obtain a precise value for t_i at a specific oxygen partial pressure (pO_2), a differential form of the above equation must be used [18]:

$$\left| \frac{dV}{d(\ln pO_2)} \right|_{pO_2'} = t_i(pO_2) \frac{kT}{4q}$$
(15)

To assist in fitting the data to the form of Eq. (15), it is convenient to have an expression which relates V to pO_2. An appropriate expression is given by [18]:

$$V = \frac{kT}{q} \left\{ \ln \left(\frac{P_p^{1/4} + \left(pO_2^I\right)^{1/4}}{P_p^{1/4} + \left(pO_2^{II}\right)^{1/4}} \right) + \ln \left(\frac{P_n^{1/4} + \left(pO_2^{II}\right)^{1/4}}{P_n^{1/4} + \left(pO_2^I\right)^{1/4}} \right) \right\}$$
(16)

where P_p and P_n are the pO_2's at which electronic transport numbers of holes and electrons are 0.5 respectively, pO_2^I is the reference pO_2, and pO_2^{II} is the working pO_2. By fitting Eq. 16 to the V versus pO_2 plot, and taking the first derivative with respective to log pO_2, the precise ionic transport number (t_i) can be obtained.

Experimental

Sample preparation

Nominally undoped and 1%Sr-doped polycrystalline langasite samples were produced using the mixed oxide route. Proportional amount of La_2O_3, Ga_2O_3, SiO_2 and $Sr(CO_3)$ (for 1%Sr doped) powders (Alfa Aesar, 99.99% metal basis) were mixed and ball milled in deionized water (without dispersant) for a day. The mixture was then dried at $110°C$ while stirred, and then uniaxially pressed into $1''$ (2.54 cm) pellets. The pellets were calcined at $950°C$ for 3 h and then sintered at $1450°C$ for 10 h. Densities achieved for undoped langasite were greater than 94% and for Sr-doped langasite


Fig. 1 Kroger-Vink diagram for acceptor doped langasite
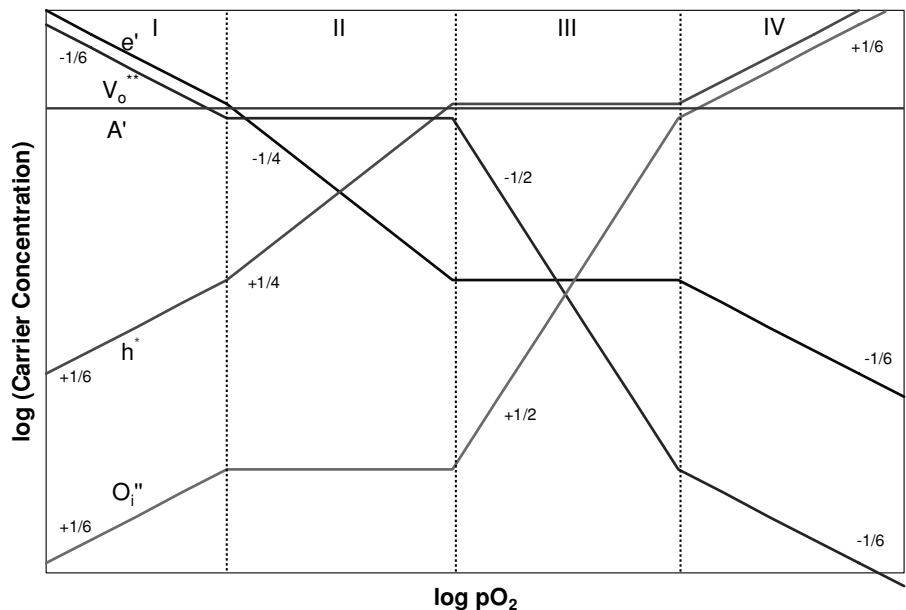
Table 1 Equations for defect species concentration in acceptor doped material

Electrical Carrier	Region I $n \approx 2[V_o^{\bullet\bullet}]$	Region II $2[V_o^{\bullet\bullet}] \approx [A_c']$	Region III $p \approx [A_c']$	Region IV $p \approx 2[O_i]$
n	$2^{1/3} pO_2^{-1/6} k_r^{1/3} \exp\left(\frac{-E_r}{3kT}\right)$	$2^{1/2} [A_c']^{-1/2} pO_2^{-1/4} k_r^{1/2} \exp\left(-\frac{E_r}{2kT}\right)$	$[A_c']^{-1} k_e \exp\left(-\frac{E_g}{kT}\right)$	$2^{-1/3} pO_2^{-1/6} k_F^{-1/3} k_o^{-1/3} k_e \exp\left(\frac{(E_o+E_F-3E_g)}{3kT}\right)$
p	$2^{-1/3} pO_2^{1/6} k_r^{-1/3} k_e \exp\left(-\frac{(E_g-1/3E_r)}{kT}\right)$	$2^{-1/2} [A_c']^{1/2} pO_2^{1/4} k_r^{-1/2} k_e \exp\left(-\frac{(E_g-1/2E_r)}{kT}\right)$	$[A_c']$	$2^{1/3} pO_2^{1/6} k_F^{1/3} k_o^{1/3} \exp\left(-\frac{(E_o+E_F)}{3kT}\right)$
$[V_o^{\bullet\bullet}]$	$2^{-2/3} pO_2^{1/6} k_r^{-1/3} k_F^{1/3} \exp\left(\frac{E_r}{3kT}\right)$	$1/2[A_c']$	$[A_c']^2 pO_2^{-1/2} k_r k_e^{-2} \exp\left(-\frac{(E_r-2E_g)}{kT}\right)$	$2^{2/3} pO_2^{-1/6} k_o^{-1/3} k_F^{2/3} \exp\left(-\frac{(2E_F-E_o)}{3kT}\right)$
$[O_i'']$	$2^{2/3} pO_2^{1/6} k_r^{-1/3} k_F \exp\left(-\frac{(E_F-1/3E_r)}{kT}\right)$	$2[A_c']^{-1} k_F \exp\left(-\frac{E_F}{kT}\right)$	$[A_c']^{-2} pO_2^{1/2} k_o k_F \exp\left(-\frac{E_o+E_F}{kT}\right)$	$2^{-2/3} pO_2^{1/6} k_F^{1/3} k_o^{1/3} \exp\left(-\frac{(E_o+E_F)}{3kT}\right)$

Fig. 2 Experimental setup for concentration cell measurements
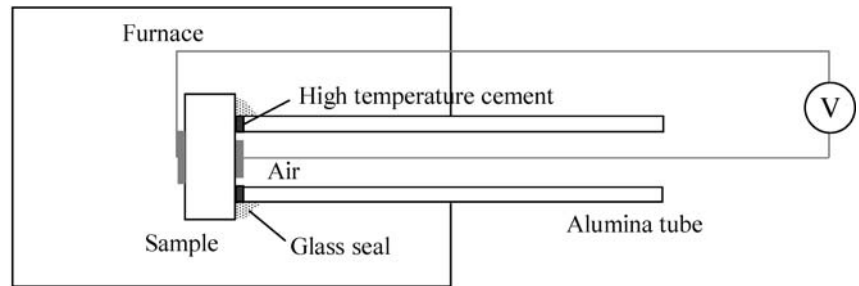
greater than 90%. No observable second phase was observed by X-ray diffraction. Pellets were cut into 2×2 mm cross sectional sample bars using a die-saw. Platinum electrodes were painted on the specimens using platinum paint from Engelhard-Clal and then fired at 850°C for 3 h.

Bulk electrical conductivity measurements

Two-point impedance measurements using a Solartron 1260 Impedance Analyzer were performed on both undoped and 1%Sr-doped langasite samples as a function of temperature and oxygen partial pressure. Measurements were made in a resistively heated tube furnace and the pO_2 was varied by using CO/CO_2 or O_2/Ar gas mixtures. Samples were allowed to equilibrate from one day (at 700°C) to 2 h (at 1000°C). Tests for reversibility were performed after measurements at low pO_2 by repeating measurements at high pO_2.

The bulk electrical conductance was extracted from the impedance spectra with the assistance of an equivalent circuit containing parallel R-C elements, one each for electrodes, grain boundaries and bulk. Conductivity values were then obtained by normalizing conductance to the appropriate geometrical factor. Note that no normalization was taken for porosity given that the undoped and Sr doped specimens exhibited densities of greater than 94 and 90% densities respectively.

Concentration cell measurements

The experimental apparatus for obtaining the ionic transport number is shown in Fig. 2. The sample, in form of a pellet, was cemented onto one end of an alumina tube using a high temperature cement (Ceramabond 569, Aremco Products Inc, Valley Cottage NY). After the cement dried overnight at room temperature, the interface was sealed against gas leakage using a glass frit dispersed in deionized water (Glass #13, Elan Technology, Midway GA), which was fired at 1000°C before measurements were performed. The experiment was performed in a tube furnace (Thermolyne 21100) with temperature varying from 700 to 1000°C (controlled by a Eurotherm 818), and the oxygen partial pressure was varied by using CO/CO_2 or O_2/Ar gas mixtures. The open circuit

voltage (V) was measured after equilibrating the setup at a set condition for 2 hrs.

The open circuit voltage was plotted as function of pO_2, and the first derivative of the plot, evaluated at various pO_2, was related to the ionic transport number via Eq. (16).

Results

The bulk electrical conductivity for both undoped and 1%Sr-doped langasite are plotted as a function of pO_2 for isotherms 700 to 1000°C at 50°C intervals in Figs. 3 and 4 respectively. For undoped langasite, the electrical conductivity is observed to be pO_2 independent at high pO_2, but becomes pO_2 dependent (n-type) under reducing conditions. This is typical behavior for a mixed ionic-electronic conductor that becomes increasingly electronic as the pO_2 decreases [12, 13]. The 1%Sr-doped langasite shows an elevated pO_2 independent conductivity with the appearance of p-type behavior at high pO_2 while the n-type conductivity is fully depressed. The addition of Sr is indicative of acceptor behavior, as successfully predicted by the defect model (Table 1).
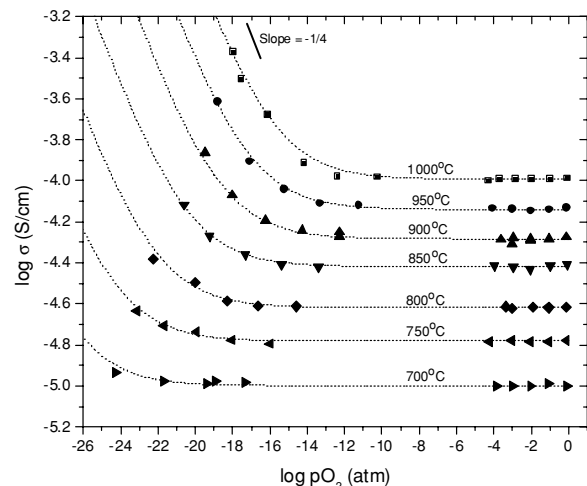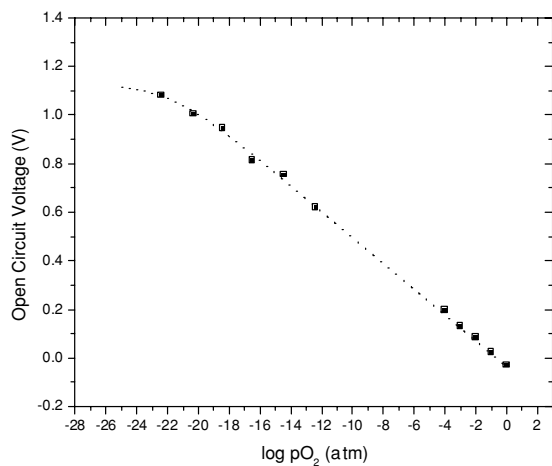

Fig. 3 Electrical conductivity vs pO_2 for nominally undoped langasite. Dotted lines are fitted values of the bulk conductivity as predicted by the defect model defect model
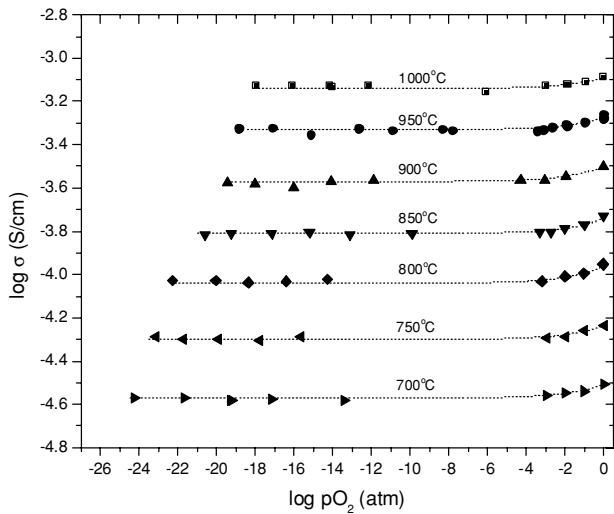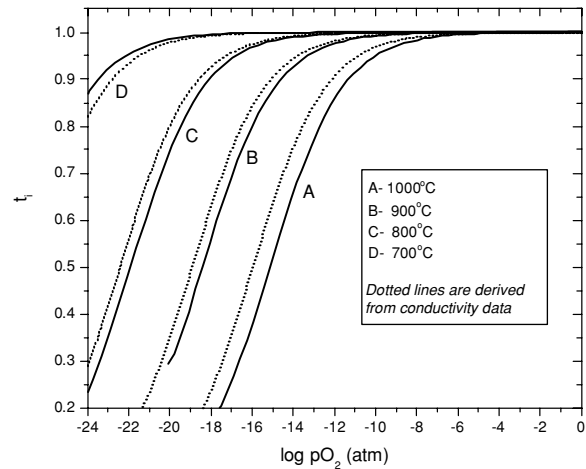
Fig. 4 Electrical Conductivity vs pO_2 for 1%Sr-doped langasite. Dotted lines are fitted values of the bulk conductivity as predicted by the defect model

The pO_2 independent regimes in Figs. 3 and 4 can be attributed, according to the defect model, to ionic conduction, in which the dominant charge carrier, the doubly charged oxygen vacancy, is charge compensated by the acceptor dopant. To verify this assumption, concentration cell measurements were performed on the nominally undoped langasite sample to determine the ionic transport number at different pO_2. The ionic transport numbers, derived from the raw open circuit voltage versus pO_2 data (example of data obtained at $800°C$ is shown in Fig. 5) and with the assistance of Eq. (15), are plotted as function of pO_2 for various temperatures (Fig. 6). Consistent with the as-derived defect model for langasite based on electrical conductivity measurements, the bulk conductivity is predominantly ionic ($t_i \approx 1$) at high oxygen partial pressures and becomes increasing electronic as pO_2 is decreased. The ionic transport numbers, derived from
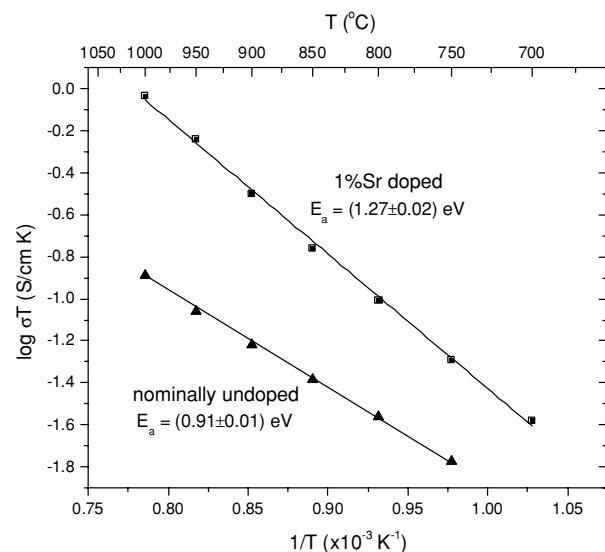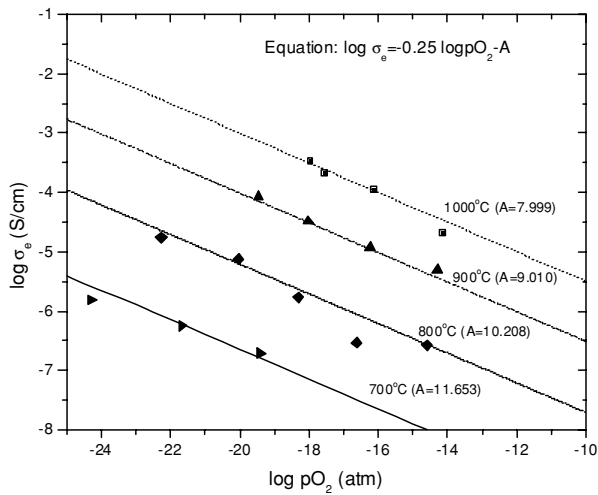

Fig. 6 Ionic transport numbers of nominally undoped langasite. Dotted lines are transport numbers derived from analysis of electrical conductivity measurements. Solid lines are data obtained from concentration cell measurements

the electrical measurements, are largely consistent with those obtained from the concentration cell measurements (Fig. 6).

The pO_2 independent ionic conductivity data for the Sr doped and undoped specimens are plotted as a function of reciprocal temperature in Fig. 7. As noted above, the Sr doped specimen exhibits a higher ionic conductivity than the nominally undoped specimen. The respective activation energies are 1.27 ± 0.02 and 0.91 ± 0.01 eV. Since the vacancy concentration is fixed by acceptors, the activation energy is expected to largely reflect the defect migration energy [12]. For high defect concentrations, an additional energy contribution from defect ordering often comes into play [19, 20]. These are discussed below, as well as the calculated ionic conductivities based on measured oxygen ion diffusivities [21].

Fig. 5 Typical open circuit voltage versus log pO_2 data for nominally undoped langasite at $800°C$. Dotted line is fitted using Eq. (15)
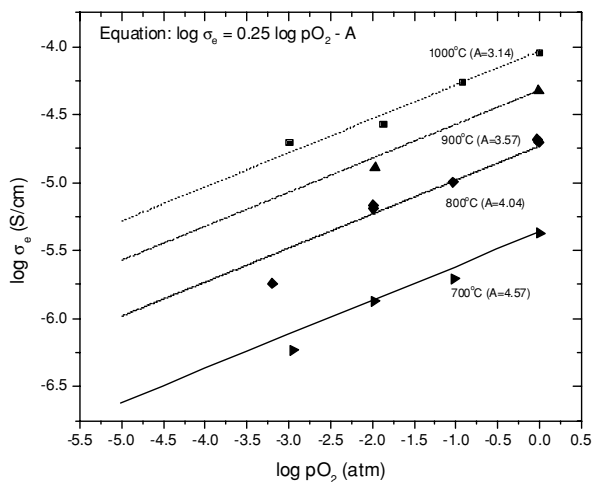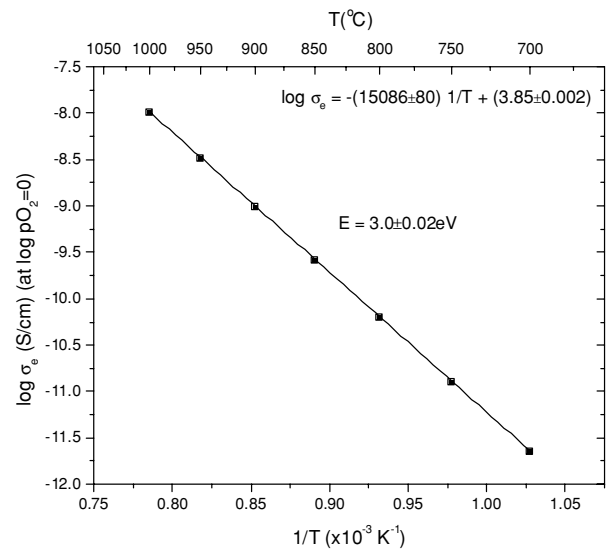

Fig. 7 Ionic conductivity of nominally undoped and 1%Sr-doped langasite

Fig. 8 N-type electronic conductivity of nominally undoped langasite as function of oxygen partial pressure

Fig. 10 Extracted n-type electronic conductivity of undoped langasite at $pO_2 = 1$ atm

The electronic components are readily deconvoluted from the total conductivity by subtracting the constant ionic from the total conductivity at each pO_2. Note that the n-type conductivity follows closely the predicted $pO_2^{-1/4}$ dependence in nominally undoped langasite (Fig. 8) and the p-type conductivity the predicted $pO_2^{+1/4}$ dependence in the Sr doped specimen (Fig. 9). The temperature dependence of the n-type and p-type conductivities evaluated at fixed pO_2 are shown in Figs. 10 and 11 respectively. The n-type conductivity is characterized by an activation energy of 3.0 ± 0.02 eV and the p-type conductivity by an activation energy of 1.09 ± 0.04 eV.

Discussion

Acceptor doped langasite was shown to be a mixed ionic-electronic conductor (Defect Region II, Fig. 1). The proposed defect model, based on acceptor compensated oxygen vacancies, was found to be consistent with both the bulk electrical conductivity data and concentration cell measurements. Both the pO_2 dependence of the total conductivity and ionic transference number and the Sr induced changes in both ionic and electronic conductivities were found to be consistent with acceptor control even in nominally undoped langasite. Given this agreement with the model, it now becomes possible to extract key thermodynamic and kinetic parameters.

Fig. 9 P-type electronic conductivity of 1%Sr-doped langasite as function of oxygen partial pressure
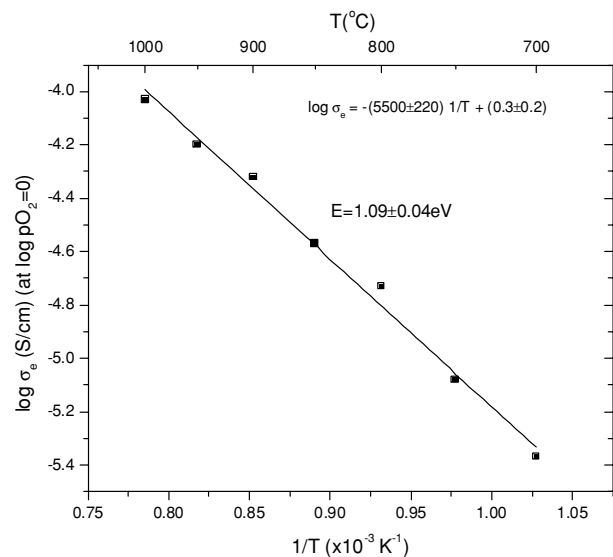
Fig. 11 p-type electronic conductivity of 1%Sr-doped langasite at $pO_2 = 1$ atm
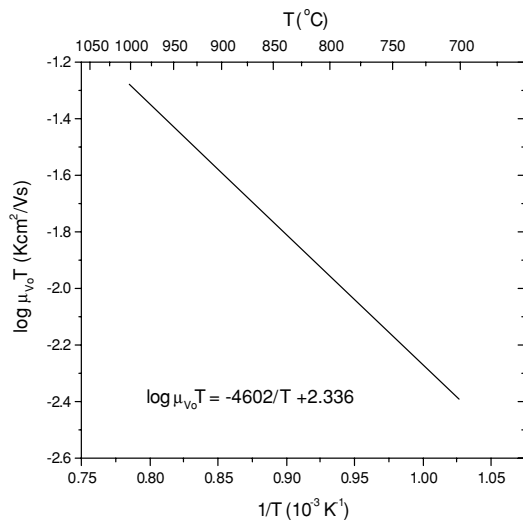
Fig. 12 Oxygen vacancy mobility-temperature product plotted as function of temperature

First, we proceed to estimate the oxygen vacancy mobility. Na was determined, by glow discharge mass spectroscopy, to be the major impurity specie in nominally undoped langasite with concentration of 1.5×10^{19} cm^{-3} (Northern Analytical Laboratory, Merrimack, NH). Na acts as an acceptor on the La site [22] and, within the ionic conductivity regime, should produce the same concentration of oxygen vacancies (according to Brouwer approximation $[Na''_{La}] \approx [V_O^{\cdot\cdot}]$). With knowledge of the ionic conductivity and the oxygen vacancy concentration, the oxygen vacancy mobility can be calculated. The oxygen vacancy mobility-temperature product is plotted as function of reciprocal temperature in Fig. 12.

Figure 12 shows that the activation energy for the oxygen vacancy mobility-temperature product is 0.91 ± 0.01 eV (equal to the activation energy of ionic conductivity-temperature product of nominally undoped langasite). The calculated oxygen vacancy mobility equation is:

$$\mu_{Vo}(T) = \frac{217}{T} \exp\left(-\frac{0.91(\pm 0.01)\,\text{eV}}{kT}\right) \text{cm}^2/\text{Vs} \quad (17)$$

The ionic conductivity activation energies were 0.91 ± 0.01 eV and 1.27 ± 0.02 eV for nominally undoped and 1%-Sr doped langasite respectively (Fig. 7). Note that the activation energy for ionic conduction in 1%Sr-doped langasite exceeds that in nominally undoped langasite by $0.36\,(\pm 0.03)$ eV (1.27 ± 0.02 vs 0.91 ± 0.01 eV). One possible explanation for the disparity between the activation energy of ionic conduction in 1%-Sr-doped and undoped samples is defect association [15, 23], in which oppositely charged defects (i.e. $V_o^{\cdot\cdot}$ and Sr'_{La}) form defect pairs such as $(Sr'_{La} - V_O^{\cdot\cdot})^{\cdot}$. Under these circumstances, only the dissociated defects contribute to conduction. One can describe the dissociation reaction by:
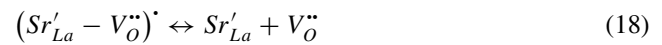
$$\left(Sr'_{La} - V_O^{\cdot\cdot}\right)^{\cdot} \leftrightarrow Sr'_{La} + V_O^{\cdot\cdot} \quad (18)$$

with the corresponding mass action relation given by:

$$K_{\text{assoc}} = \frac{[Sr'_{La}]\,[V_O^{\cdot\cdot}]}{\left[(Sr'_{La} - V_O^{\cdot\cdot})^{\cdot}\right]} = k_{\text{assoc}} \exp\left(-\frac{E_{\text{assoc}}}{kT}\right) \text{cm}^{-3} \quad (19)$$

The following mass conservation law applies:

$$[Sr_{\text{total}}] = [Sr'_{La}] + \left[(Sr'_{La} - V_O^{\cdot\cdot})^{\cdot}\right] \quad (20)$$

The following electroneutrality also applies:

$$[Sr'_{La}] = 2\left[V_O^{\cdot\cdot}\right] + \left[(Sr'_{La} - V_O^{\cdot\cdot})^{\cdot}\right] \quad (21)$$

Substituting Eq. (20) into Eq. (19), gives:

$$K_{\text{assoc}} = \frac{[V_O^{\cdot\cdot}]\,[Sr'_{La}]}{[Sr_{\text{total}}] - [Sr'_{La}]} = k_{\text{assoc}} \exp\left(-\frac{E_{\text{assoc}}}{kT}\right) \quad (22)$$

It is useful to examine the predictions of this model at the extremes of low and high temperature, i.e., for very low dissociation and nearly full dissociation. For a high degree of association at low temperatures, based on Eq. (21):

$$[Sr'_{La}] \cong \left[(Sr'_{La} - V_O^{\cdot\cdot})^{\cdot}\right] \quad (23)$$

Substituting this expression into Eq. (19) results in the following expression for the unassociated oxygen vacancy concentration (see Regime III in Fig. 13):

$$[V_O^{\cdot\cdot}] = k_{\text{assoc}} \exp\left(-\frac{E_{\text{assoc}}}{kT}\right) \quad (24)$$

On the other hand, at high enough temperature, dissociation becomes nearly complete (Regime I in Fig. 13) and then Eq. (21) becomes:

$$[Sr'_{La}] = 2\left[V_O^{\cdot\cdot}\right] \cong [Sr_{\text{total}}] \quad (25)$$

Thus, the vacancy concentration is predicted to shift from an activated process at low temperature to a constant value at high temperature. In the transition from the low to high temperature regime, one expects to observe curvature in the $\log[V_O^{\cdot\cdot}]$ vs 1/T plot (Regime II in Fig. 13).
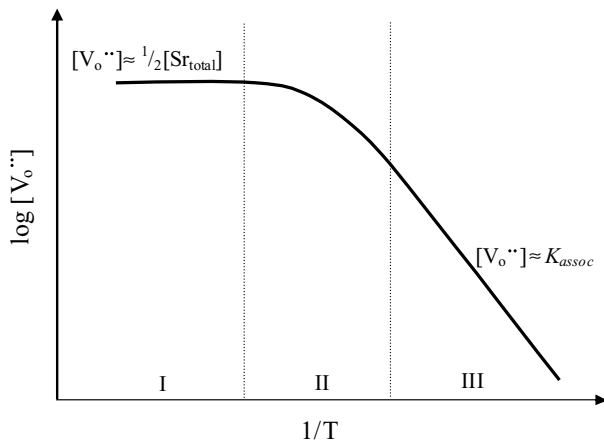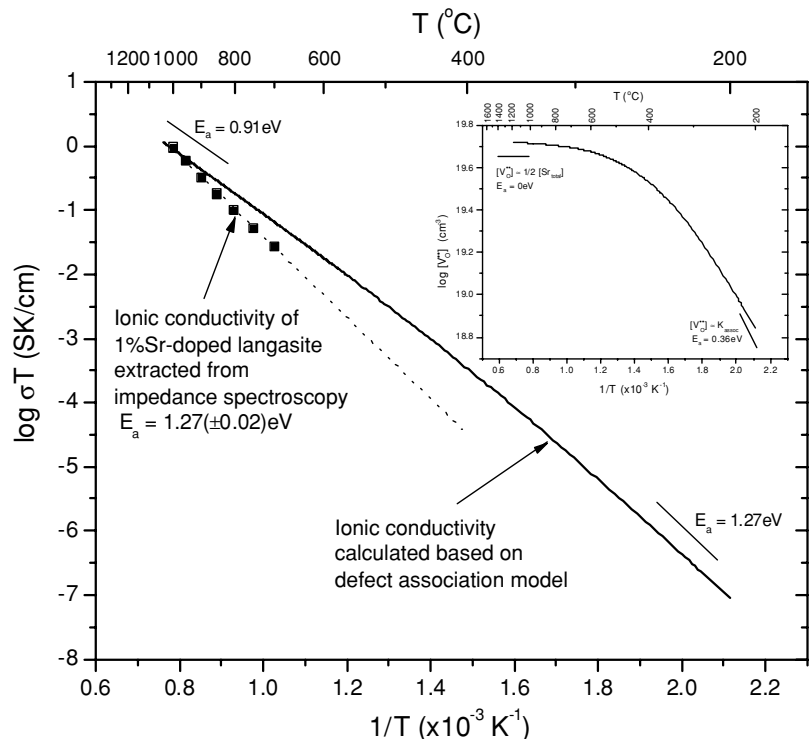
Fig. 13 Dissociated oxygen vacancy concentration as function of reciprocal temperature. In Regime I, defects are nearly completely dissociated while in Regime III, defects are nearly fully associated

The disparity between the activation energy of ionic conduction in 1%Sr-doped and undoped langasite (1.27 ± 0.02 vs 0.91 ±0.01 eV) could in principle be attributed to defect association as discussed above. Indeed, we can calculate the ionic conductivity of 1%Sr-doped langasite assuming that defect association is the correct explanation for the larger activation energy. To do that, we define x as:

$$x = \frac{[V_O^{\cdot\cdot}]}{[Sr_{total}]} \qquad (26)$$

Using Eq. (20) and (21):

$$x + \frac{1}{2} = \frac{[Sr'_{La}]}{[Sr_{total}]} \qquad (27)$$

Substituting Eqs. (26) and (27) into Eq. (22):

$$K_{assoc} = \frac{x\left(x + \frac{1}{2}\right)}{\frac{1}{2} - x}[Sr_{total}] = k_{assoc} \exp\left(-\frac{E_{assoc}}{kT}\right) \qquad (28)$$

The pre-exponential k_{assoc} is defined as the product of degree of freedom of the defect pair and the number of oxygen lattice sites in langasite ($\sim 2.14 \times 10^{23}$ cm^{-3}) [15, 17, 23], and E_{assoc} is 0.36($\pm$ 0.03) eV, which is the difference in activation energy for ionic conductivity between 1%Sr-doped and nominally undoped langasite. Solving Eq. (28) gives us the concentration of unassociated oxygen vacancies (see insert, Fig. 14) and, with the oxygen mobility derived in Eq. (17), the ionic conductivity that is based on defect association model can be calculated (Fig. 14). From Fig. 14, it can be seen that for the temperature range examined in the conductivity measurements (700–1000°C), the defect pairs would be largely dissociated (Regime I in Fig. 13) and the activation energy should only reflect the oxygen vacancy migration energy (0.91 eV). In order to observe E_{assoc} of 0.36 eV (for a total activation energy of 1.27 eV as seen in the case of 1%Sr-doped langasite), its conductivity would have to be measured at temperatures below 300°C. Therefore, defect association

Fig. 14 Ionic conductivity of 1%Sr-doped langasite – comparison between extracted values from impedance spectroscopy and calculated values (insert shows calculated $[V_O^{\cdot\cdot}]$), assuming a defect association model

cannot explain the disparity between the activation energy of ionic conduction in 1%Sr-doped and undoped langasite.

An alternative explanation, taking into account the failure of the dilute solution approximation at the 1% Sr level, is next discussed. For concentrated solutions, long range defect interactions must be taken into account. Wang et al [19], for example, observed that the activation energy for oxygen ion conductivity in Y_2O_3 doped CeO_2 increased systematically as the yttrium content increased from 1 to 40 mol%. In a number of fluorite and pyrochlore systems [20, 24, 25], this has been attributed to long range defect ordering which effectively traps the defects in deeper potential wells to overcome as they move through the lattice. This would explain the higher activation energy observed for ionic conductivity in 1%Sr-doped langasite as compared to nominally undoped langasite which more reasonably remains in dilute solution.

In order to independently verify that oxygen ions dominate the ionic conductivity, Schulz et al [21], using oxygen tracer exchange and SIMS concentration profiling, obtained values for the oxygen self diffusivity of 1%Sr-doped and undoped langasite samples prepared in this laboratory. While they found an activation energy of oxygen self diffusivity in the range of 1.2 ± 0.2 eV for the langasite specimens, in reasonable agreement with the values reported above for the conductivity measurements, they were inverted in order, i.e. 1.39 eV for undoped and 0.96 eV for the doped specimen. While the diffusivity data are in qualitative agreement with the findings from the conductivity and concentration cell measurements, i.e., a significant contribution to electrical transport by oxygen ions, precise quantitative agreement is lacking. This may be related to difficulties with the diffusion measurements as described in [21]. In addition, Ga tracer diffusion measurements were performed on single crystal langasite, demonstrating that self-diffusivity of Ga is many orders of magnitude lower than that of oxygen.

Turning to the electronic conductivity, it should be possible to extract values for E_r and E_O from the activation energies characterizing the n and p type conductivities respectively (see equations listed under Region II, Table 1). According to the defect model for acceptor-doped langasite, the activation energy for electron generation (n-type conductivity) equals $\frac{1}{2}E_r$ (half of reduction enthalpy) plus the electron migration energy E_{μ_e}. From studies on donor-doped langasite, we learned that electrons migrate by an activated mechanism, with an activation energy of 0.15 ± 0.01 eV [10]. This leads to values of $E_r = 5.7 \pm 0.06$ eV. Similarly, the activation energy for hole generation (of p-type conductivity) equals $\frac{1}{2}E_o$ (half of oxidation enthalpy) plus the hole migration energy E_{μ_e}. Since we have no independent information, we will assume that holes move through the lattice in a nonactivated manner, and thus the oxidation enthalpy is given as $E_o = 2.18 \pm 0.08$ eV. Next the thermal bandgap can be calculated from Eq. (10), i.e. $E_g = 3.94 \pm 0.07$ eV. The

optical bandgap of single crystal langasite reported by Dubovik et al. [26] was ~4.5 eV, in reasonably good agreement with the value derived in this study.

Referring to Table 1, K_r can be extracted from knowledge of the temperature dependence of n at a given pO_2 and dopant level (i.e. in Region II). Beginning with values for n (i.e. electron mobility and conductivity known – Fig. 10) and known dopant level, K_r for acceptor-doped langasite was calculated:

$$K_r = 10^{67} \exp\left(-\frac{5.7 \pm 0.06 \, eV}{kT}\right) \text{cm}^{-9} \text{atm}^{0.5} \qquad (29)$$

And as k_r is now known from Eq. (29), and k_e is simply $N_v N_c$, where N_v and N_c are the density of states for hole and electron respectively, k_o can be subsequently determined from Eq. (11).

With the hole mobility assumed to be nonactivated, it follows that the semiconductor model for the density of states (as described in, for example, [14]) can be applied (Eq. (12)). Using the equation, N_v can be estimated (assuming $m_h^* \approx 2$ and $T \approx 1000$ C) to be about 4×10^{20} cm^{-3}. The electron mobility in langasite is activated and is described by polaron hopping [10]. The density of states for electrons is also calculated in [10] and is given as $N_c = 8.9 \times 10^{19}$ cm^{-3}.

The value for k_e ($= N_c N_v$) is calculated to be 3.6×10^{40} cm^{-6} and k_o can be estimated to be 1.3×10^{14} cm^{-3}atm$^{-0.5}$. K_o for acceptor-doped langasite is then:

$$K_O = 1.3 \times 10^{14} \exp\left(-\frac{2.18 \pm 0.08 \text{ eV}}{kT}\right) \text{cm}^{-3} \text{ atm}^{-0.5}$$

$$(30)$$

The hole density, p, can be determined using Eqs. (4) and (30). Since the hole conductivity of 1%Sr-doped langasite is known, the hole mobility can be calculated and is found to be ~120 cm^2/V·s, decreasing slightly with increasing temperature. The negligible dependence on temperature for the hole mobility is consistent with the initial assumption of a non-activated mobility. The value of ~120 cm^2/V·s is considered high for hole conduction in oxide materials but still plausible [27].

Table 2 summarizes the results obtained for acceptor doped langasite. From these results, the concentrations of the major defect species (i.e. oxygen vacancies, electrons and holes) and their electrical mobilities can be calculated and consequently the bulk conductivity can be predicted as

Table 2 Summary of results

K_r (cm^{-9} atm$^{0.5}$)	$K_r = 10^{67} \exp\left(-\frac{5.7 \pm 0.06 \text{ eV}}{kT}\right)$
K_o (cm^{-3} atm$^{-0.5}$)	$K_O = 1.3 \times 10^{14} \exp\left(-\frac{2.18 \pm 0.08 \text{ eV}}{kT}\right)$
K_e (cm^{-6})	$K_e = 6.8 \times 10^{42} \exp\left(-\frac{3.94 \pm 0.07 \text{ eV}}{kT}\right)$
μ_h (cm^2/Vs)	$\mu_h \approx 120$
μ_{Vo} (cm^2/Vs)	$\mu_{Vo} = \frac{217}{T} \exp\left(-\frac{0.91 \pm 0.01 \text{ eV}}{kT}\right)$

function of dopants, temperatures and pO_2 (see dotted curves in Figs. 3 and 4).

Conclusions

Acceptor doped langasite was found to exhibit mixed ionic-electronic conductivity behavior. At high pO_2, nominally undoped (with background acceptors) langasite was a predominantly ionic conductor due to mobile oxygen vacancies. The ionic conductivity was pO_2-independent and fixed by background acceptors. At low pO_2, the conductivity becomes increasingly n-type electronic dominated by electrons generated by reduction. Increasing the acceptor dopant level, by adding strontium on lanthanum sites, increase the ionic and p-type electronic conductivity, while fully depressing the n-type electronic conductivity – observations consistent with predictions of the defect model based on oxygen vacancies, formed to compensate extrinsic acceptor impurities, being the dominant defect

Sr-doped langasite was found to have a higher activation energy for oxygen transport (1.27 ± 0.02 eV) than nominally undoped langasite (1.27 ± 0.02 eV). This difference could not be successfully explained by applying a simple defect association model but required the assumption of long range defect interactions.

Using the defect model, a number of key equilibrium constants and defect mobilities were derived as summarized in Table 2.

References

1. J.W. Mrosk, C. Ettl, L. Berger, P. Dabala, H.J. Fecht, G. Fischerauer, J. Hornsteiner, K. Riek, E. Riha, E. Born, W. Werner, A. Dommann, J. Auersperg, E. Kieselstein, B. Michel, and A. Mucha, *SAW sensors for high temperature applications. Proceedings of 24th Annual Meeting of IEEE Industrial Electronics Society*, IECON 1998, 1998: p. 2386–2390.
2. D. Damjanovic, Materials for high temperature piezoelectric transducers, *Current Opinion in Solid State & Materials Science*, **3**, 469–473 (1998).
3. R. Mital, J. Li, S.C. Huang, B.J. Stroia, and R.C. Yu, *Diesel exhaust emissions control for light duty vehicles.* SAE Technical Paper Series (2003-01-0041), 2003.
4. M.S. Brogan, A.D. Clark, and R.J. Brisley, *Recent progress in NOx trap technology.* SAE Technical Paper Series (980933), 1998.
5. Y.-W. Kim, J. Sun, I. Kolmanovsky, and J. Koncsol, *A phenomenological control oriented lean NOx trap model.* SAE Technical Paper Series (2003-01-1164), 2003.
6. H. Fritze, H.L. Tuller, H. Seh, and G. Borchardt, High temperature nanobalance sensor based on langasite. *Sensors and Actuators B*, **76**, 103–107 (2001).
7. H. Seh, H.L. Tuller, and H. Fritze, Langasite for high-temperature acoustic wave gas sensors, *Sensors and Actuators B*, **93**, 169–174 (2003).
8. H. Seh, H.L. Tuller, and H. Fritze, Electrical conductivity prediction in langasite for optimized microbalance performance at elevated temperatures, *Proceedings of MRS Symposium* **756**, 175–180 (2003).
9. H. Seh, H.L. Tuller, and H. Fritze, Defect properties of langasite and effects on BAW gas sensor performance at high temperatures, *J. European Ceramic Society*, **24**, 1425–1429 (2004).
10. H. Seh and H.L. Tuller, Defect chemistry of donor-doped langasite. *Submitted to Journal of Electroceramics* (2004).
11. H. Seh, H.L. Tuller, and H. Fritze, Impact of defect chemistry on langasite resonator operations at high temperatures, *Submitted to J. Electroceram.* (2004).
12. S.R. Rotman, R.P. Tandon, and H.L. Tuller, Defect-property correlations in garnet crystals: the electrical conductivity and defect structure of luminescent cerium-doped yttrium aluminum garnet, *J. Appl.Phys.*, **57**(6), 1951–1955 (1984).
13. S.R. Rotman, H.L. Tuller, M. Roth, and A. Linz, Defect property correlations in garnet crystals. II. Electrical conductivity and optical absorption in $Ca_3Al_2Ge_3O_{12}$, *J. Appl. Phys.*, **57**(12), 5320–5324 (1985).
14. N.W. Ashcroft and N.D. Mermin, *Solid State Physics* (Saunders College Publishing, 1976).
15. W.D. Kingery, H.K. Bowen, and D.R. Uhlmann, *Introduction to Ceramics*. (John Wailey & Son, 1976).
16. Y.-M. Chiang, D.B. III, and W.D. Kingery, *Physical Ceramics* (John Wiley & Sons, Inc, 1997).
17. D.M. Smyth, *The Defect Chemistry of Metal Oxides* (Oxford University Press, 2000).
18. H.L. Tuller, *Mixed conduction in nonstoichiometric oxides*, in *Nonstoichiometric Oxides*, O.T. Sorensen (ed.). (Academic Press, New York, 1981), p. 271–335.
19. D.Y. Wang, D.S. Park, J. Griffith, and A.S. Nowick, Oxygen-ion conductivity and defect interactions in yttria-doped ceria, *Solid State Ionics*, **2**, 95–105 (1981).
20. H.L. Tuller, Oxygen ion conduction and structural disorder in conductive oxides, *J. Physi. and Chemis. Sol.*, **55**(12), 1393–1404 (1994).
21. M. Schulz, H. Fritze, H.L. Tuller, and H. Seh, Diffusion related implications for langasite resonator operation, *IEEE Transactions on Ultrasonics, Ferroelectrics, and Frequency Control*, **51**(11), 1381–1387 (2004).
22. B.V. Mill and Y.V. Pisarevsky, Langasite-type materials: from discovery to present state, *IEEE/EIA International Frequency Control Symposium and Exhibition*, 133–144 (2000).
23. R. Merkle and J. Maier, Defect association in acceptor-doped $SrTiO_3$: Case study for $Fe'_{Ti}V_0$ and $Mn_{Ti}''''V_0$, *Physical Chemi. Chem. Phys.*, **5**(11), 2297–3303 (2003).
24. S.A. Kramer and H.L. Tuller, A novel titanate-based oxygen ion conductor: $Gd_2Ti_2O_7$, *Solid State Ionics, Diffusion & Reactions*, **82**(1-2), 15–23 (1995).
25. Y. Taehwan and H.L. Tuller, Ionic conduction and disorder in the $Gd_2Sn_2O_7$ pyrochlore system, *Solid State Ionics, Diffusion & Reactions*, **86–88**(1), 177–182 (1996).
26. M.F. Dubovik, K.A. Katrunov, and T.I. Korshikova, The nature of langasite crystal's coloration, *IEEE International Frequency Control Symposium*, 638–641 (1995).
27. T. Minami, New n-type transparent conducting oxides, *MRS Bulletin*, **25**, 38–44 (2000).